Materials Advances

ROYAL SOCIETY OF CHEMISTRY

PAPER

View Article Online
View Journal | View Issue

Cite this: *Mater. Adv.*, 2025, 6, 5605

Rapid detection of mercury ions in water using functionalized liquid crystal microdroplets†

Saumya Ranjan Pradhan, Krishnakanth Chithari, Ramadevi Suguru Pathinti and Jayalakshmi Vallamkondu *

Received 21st March 2025,
Accepted 17th June 2025

DOI: 10.1039/d5ma00260e

rsc.li/materials-advances

In this study, we present a stimuli-responsive liquid crystal (LC) droplet-based sensor system coated with poly(ethylene imine) (PEI) and Tween-20 for the detection of mercury ions (Hg^{2+}) in aqueous environments. Upon exposure to Hg^{2+}, the LC droplets undergo a distinct orientational transition from radial (homeotropic) to bipolar (planar), which can be clearly visualized using polarized optical microscopy (POM). This response is attributed to the strong interaction between mercury ions and the amine groups present in the PEI coating. The sensor exhibits a rapid response time of approximately 10 s at a mercury ion concentration as low as 59 mM. The limit of detection (LOD) in distilled water is determined to be 4.71 mM using a sample volume of 160 μL. The sensitivity of the system is influenced by parameters such as the concentration and volume of the mercury ion solution and the number of LC droplets used. Furthermore, the sensor demonstrates reliable detection of Hg^{2+} in various water samples, including distilled and lake water, indicating its practical applicability. In addition to detection, the PEI/Tween-20-coated LC droplets show potential for reducing mercury ion concentration through surface adsorption. This approach offers a simple, cost-effective alternative to conventional instrumentation for on-site mercury detection in environmental samples.

1. Introduction

Water contamination by heavy metal ions has posed a severe global problem for decades. Heavy metals become highly toxic when they bind with protein thiol groups, leading to cellular penetration where they can cause oxidative damage, disrupt biological functions, and even lead to cancer. Among various metal ions, mercury (Hg^{2+}) is recognized as one of the most toxic, particularly in environmental contexts, often resulting in significant water pollution. Freshwater bodies like lakes and rivers can accumulate high levels of Hg^{2+}, which, through the food chain, can be readily absorbed by humans. Exposure to Hg^{2+} can lead to serious immune system impairment and organ damage. The accumulation of Hg^{2+} in the body is linked to conditions such as acrodynia, Minamata disease,[1] and Hunter–Russell syndrome,[2] along with irreversible harm to the kidneys,[3] brain, and nervous system, which may ultimately result in fatality.[4,5] Traditional methods for quantifying Hg^{2+} ions include atomic fluorescence spectroscopy,[6,7] mass spectrometry,[8] atomic plasma spectroscopy,[9] and Raman spectroscopy.[10] These procedures require sophisticated instrumentation and are often labour-intensive, hence generating a need for more speed, simple, and economical detection methods. DNA duplexes with T–T mismatches display a higher binding affinity for Hg^{2+} than A–T pairs, indicating their capacity to selectively sequester Hg^{2+} and establish stable T–Hg^{2+}–T complexes, as documented by Ono and Togashi (2004).[11] Techniques employing this T-rich DNA mechanism, such as electrochemistry,[12] luminescence,[13,14] colorimetric assays,[15] and Raman scattering,[16] have demonstrated notable selectivity and stability in the detection of Hg^{2+}.

Polyethyleneimine (PEI) is a water-soluble polymer known for its ability to selectively complex metal ions, a property recognized early on. Extensive research has explored its diverse applications, including use in the nuclear industry and in the removal of toxic heavy metal ions such as Pb(II), Cd(II), and Hg(II). As advancements in ligand design have yielded increasingly complex and selective complexing agents, attaching these reagents to polymer backbones has emerged as a promising approach to minimize the loss of costly compounds.[17] Notably, PEI exhibits a higher absorption capacity for Hg^{2+} ions compared to Mn^{2+} and Cd^{2+} ions.[18]

Liquid crystals (LCs) have lately exhibited promise as innovative sensing systems.[19–21] The orientation of liquid crystal (LC) molecules is very susceptible to chemical and molecular interactions because of their extensive orientational order, resulting in enhanced optical signals.[22,23] LC-based sensors

Department of Physics, National Institute of Technology, Warangal 506004, India. E-mail: jayalakshmiv@nitw.ac.in

† Electronic supplementary information (ESI) available. See DOI: https://doi.org/10.1039/d5ma00260e

enable detection in ambient light without requiring electrical current or chemical tagging, generating optical signals visible to the naked eye. These characteristics make LC-based sensors ideal for applications requiring cost-effectiveness, high sensitivity, direct transduction, and simple detection.[24–30] A variety of biological and chemical compounds, such as DNA,[31–33] proteins,[34–40] enzymes,[41,42] proteases,[43,44] viruses,[45,46] and other analytes[47–60] have been detected using LC-based sensors. Research has examined liquid chromatography techniques for the identification of heavy metals. Hu *et al.* developed a liquid crystal (LC)-based sensor employing surface-immobilized urease to detect Cu^{2+} ions in aqueous solutions, leading to a transition in the LC's optical response from bright to dark due to urease inhibition by Cu^{2+} ions.[61] Similarly, Jang *et al.* utilized 4-cyano-4-pentyl biphenyl (5CB) infused with stearic acid to detect Cu^{2+} and Co^{2+} ions by monitoring optical changes in liquid crystal alignment at the aqueous interface.[62]

Recent advancements include LC-based methods for the detection of Hg^{2+} ions in aqueous solutions. Yang *et al.* created an LC biosensor utilizing oligonucleotide probes that modified LC orientation upon interaction with Hg^{2+}, due to of oligonucleotide unique property to bind specifically to two DNA thymine (T) bases, is used as a model heavy metal ion.[63] Chen *et al.* developed an LC-based biosensor for the detection of mercury ions by using ligand-doped liquid crystal. The mercury ion is detected as a result of the interaction between the complex of ligand and Hg^{2+} formation.[64] Singh *et al.* developed a liquid chromatography-based sensor incorporating amphiphilic dithiocarbamate for the selective detection of Hg^{2+}, It will be detected by LC as a result of the dithiocarbamate chelating group of MeDT with Hg^{2+} ion at the aqueous interface, which disrupted the orientation of LCs and produced a brilliant texture.[65]

Hong *et al.* utilized aptamers in a liquid chromatographic sensor for the selective detection of Hg^{2+} ions. This sensor is based on interactions between trimethyl octadecyl ammonium bromide (OTAB) and Hg^{2+}-binding aptamer.[66] Here we hypothesize that Hg^{2+} ions can be selectively and sensitively detected using nematic liquid crystal (NLC) droplets stabilized with polyethyleneimine (PEI) and Tween-20, without the need for oligonucleotides or other molecular recognition elements. Unlike previous LC-based sensors that require DNA probes or functionalized ligands for specificity, our simplified LC-based sensor design specifically detected Hg^{2+} ions in actual water sample (tap water) without doping oligonucleotide.

This study involved the generation of monodispersed nematic liquid crystal (NLC) droplets stabilized by a polyethyleneimine (PEI) and Tween-20 surfactant layer, enhancing droplet stability. Our research group previously utilized liquid crystal droplets stabilized with polyvinyl alcohol (PVA)/$SC_{12}S$ for the detection of bile acids and bovine serum albumin (BSA)[39,67] and developed an economical method for the early detection of Alzheimer's disease using PEI/Tween-20 stabilized liquid crystal droplets.[68] We utilized PEI/Tween-20 coated LC droplets for the selective detection of Hg^{2+} ions in aqueous solutions. Due to the interaction between Hg^{2+} and the amine groups on PEI induces structural changes in the LC droplets, transitioning them from a homeotropic to planar configuration. These changes, observable under a polarized optical microscope (POM), allow Hg^{2+} ion detection by monitoring the transition from hedgehog (radial) to boojum (bipolar) configurations within fraction of the seconds. This label-free, simple, and cost-effective optical probe enables reliable detection of Hg^{2+} ions in aqueous solutions.

2. Experimental

2.1 Materials

Nematic liquid crystal E7 was purchased from Merck. Polyethyleneimine (PEI, 50 wt%), polyvinyl alcohol (PVA, molecular weight ~160 000, HIMEDIA), sodium dodecyl sulfate ($SC_{12}S$, molecular weight ~288.38, SRL), cetyltrimethylammonium bromide (CTAB, extrapure AR, 99%, molecular weight ~364.45, SRL), coumarin 6 (98%, CAS no. 38215-36-0, Sigma-Aldrich), Tween-20, mercury(II) chloride ($HgCl_2$), magnesium chloride ($MgCl_2$), calcium chloride ($CaCl_2$), ferrous chloride ($FeCl_2$), zinc chloride ($ZnCl_2$), cadmium chloride ($CdCl_2$), copper chloride ($CuCl_2$), and sodium chloride (NaCl) were obtained from Sigma-Aldrich. PEI with amine groups was also purchased from Sigma-Aldrich. Additionally, Tween-20, lead nitrate, and all solvents were procured from SRL Chemicals. All reagents were of analytical grade and used without further purification.

2.2 Fabrication of flow-focusing microfluidic device

The flow-focusing microfluidic device was employed to produce monodispersed LC droplets. To construct this device, a tapered cylindrical capillary (inner diameter 0.58 mm, outer diameter 1.0 mm; borosilicate glass) was inserted into a square capillary (inner diameter 1.0 mm, wall thickness 0.2 mm; Square-Boro Tubing), as illustrated in Fig. 1. The left end of the cylindrical capillary was tapered using a Flaming micropipette puller (P-97, Sutter Instrument), and then precisely sanded to a 40 μm orifice with a Microforge (MF-830, Narishige). All capillaries were blown with air and rinsed with water to remove dust particles. Octadecyl trimethoxy silane (OTS) was applied to render the square capillary hydrophobic. The treated square capillary was then fitted with the tapered cylindrical capillary, and two needles were epoxy-glued to each end of the square capillary to facilitate fluid pumping without leakage.

2.3 Preparation of metal ion solutions

To investigate the response times as a function of mercury ion concentration, a series of mercury ion solutions were prepared in both distilled waters, tap water and lake water. Concentrations were varied systematically, including 4.71 mM, 8 mM, 9.8 mM, 10.31 mM, 14.8 mM, 22.1 mM, 29.6 mM, 36.9 mM, 44.2 mM, 51.6 mM, and 59 mM. This range of concentrations allowed for a thorough assessment of the sensor's responsiveness across varying mercury levels, offering valuable insights into how concentration influences the sensor's detection

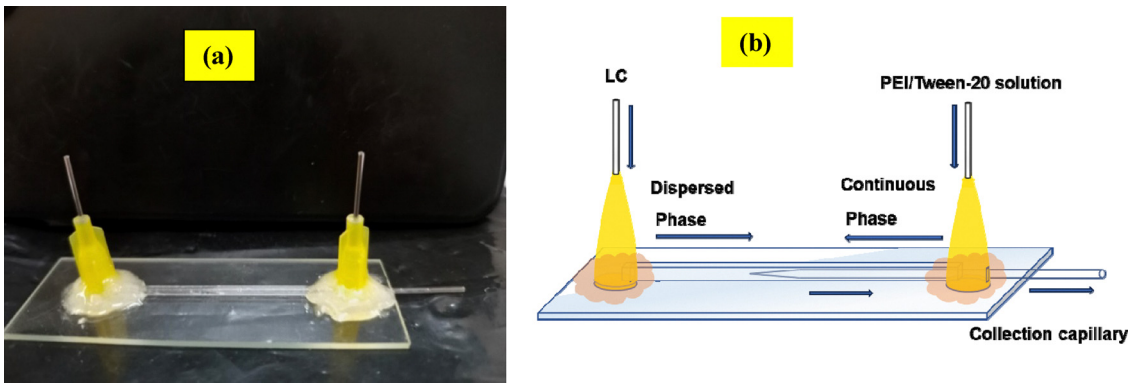

Fig. 1 (a) Photograph of the flow-focusing microfluidic device. (b) Schematic diagram illustrating the direction of fluid flow within the microfluidic device.

efficiency and response behavior in distilled water, tap water and lake water.

2.4 Characterization

A polarizing optical microscope (POM) (Olympus BX53, USA) in transmission mode, equipped with a CCD camera (Micropublisher RTV 5.0, Q-Imaging), was used to analyze the director arrangement of the liquid crystal (LC) within the droplets and capture textural images of the LC. Additionally, a fluorescence microscope (Olympus IX 73 inverted microscope, Japan) was employed to observe fluorescence images on the surface of the LC droplets. Chemical composition was assessed through Raman spectroscopy, with spectra recorded using an in Via Raman 785 ER system featuring a 785 nm laser and a charge-coupled device (CCD) detector, provided by Wasatch Photonics.

2.5 Detection of mercury ion (Hg^{2+}) in aqueous environments

To detect mercury ions, a 4 μL droplet of the $LC_{PEI/Tween\text{-}20}$ emulsion was carefully deposited onto a clean glass slide. Different concentrations of mercury ions (Hg^{2+}) were then introduced to observe the response time of the $LC_{PEI/Tween\text{-}20}$ droplets as they transitioned from a homeotropic to a planar configuration. This procedure was repeated for each concentration to ensure consistency and accuracy in the measurements.

3. Results and discussion

3.1 Selection of surfactants for mercury ion (Hg^{2+}) detection

We investigated different surfactant combinations (PVA/$SC_{12}S$, PVA/CTAB, and PEI/Tween-20) to produce LC droplets using a vortex mixer, assessing their responsiveness to mercury ions (Hg^{2+}) to identify the optimal surfactant for Hg^{2+} detection. Initially, LC droplets coated with PVA (1 wt%)/$SC_{12}S$ (5 mM) were prepared, displaying a radial structure under a polarized optical microscope (POM). Upon immersing these LC droplets in an aqueous Hg^{2+} solution, their orientation shifted from radial to bipolar, visible under POM after approximately 10 min, as shown in Fig. 2. In the absence of Hg^{2+} ions, no structural transition was observed in the LC droplets. The Hg^{2+} solution was prepared in a buffer at pH 4.

We observed that LC droplets in tap water transitioned from homeotropic (radial) to planar (bipolar) alignment, irrespective of the presence of mercury ions. The observed behaviour is probably attributable to the pH sensitivity of the PVA/$SC_{12}S$ surfactant coating,[39] resulting in orientation alterations in

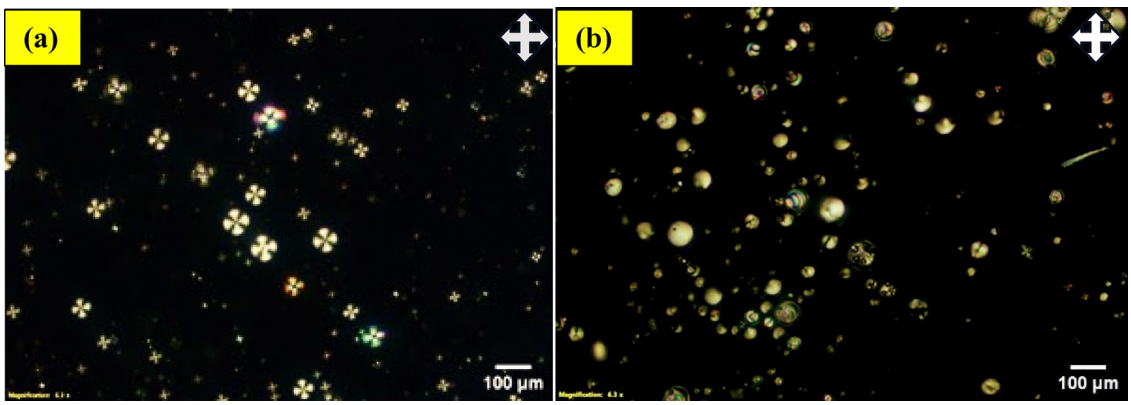

Fig. 2 POM images of LC droplets coated with PVA (1 wt%)/$SC_{12}S$ (5 mM): (a) before and (b) after the addition of Hg^{2+} ions (59 mM) in a buffer solution at pH 4.

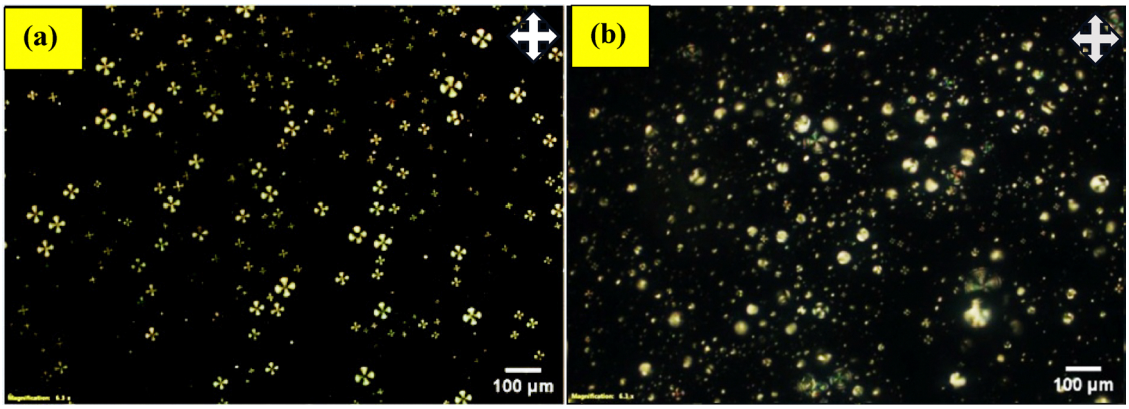

Fig. 3 POM pictures of LC droplets coated with PVA (1 wt%)/CTAB (5 mM): (a) prior to and (b) subsequent to the introduction of Hg^{2+} ions (59 mM) in a buffer solution at pH 4.

the droplets. Consequently, these droplets can only identify mercury ions in a buffer solution, but not in tap water. We additionally examined LC droplets coated with PVA (1 wt%)/CTAB (5 mM) and observed that they exhibited a comparable response to mercury ions in a buffer solution, akin to PVA/$SC_{12}S$-coated droplets. This indicates that PVA/CTAB-coated droplets proficiently identify mercury ions in the buffer, shifting from homeotropic to planar alignment within 10 min, as depicted in Fig. 3.

The LC droplets preserved a radial configuration even without the presence of mercury ions.

In tap water, the LC droplets transitioned from a homeotropic to a planar orientation, irrespective of the presence of mercury ions. To enable mercury ion detection in tap water, we tested LC droplets coated with PEI and Tween-20 in distilled water and buffer solutions. A rapid orientation changes from homeotropic (radial) to planar (bipolar) was observed within a few seconds (10 s), as shown in Fig. 4. Of the three surfactants tested, PEI/Tween-20-coated LC droplets proved most effective for detecting mercury ions in buffer solutions, distilled water, tap water (real water samples) and lake water. Therefore, we selected PEI (1 wt%)/Tween-20 (0.05 wt%) as the surfactant for mercury ion detection in aqueous solutions.

3.2 Production of monodispersed LC droplets and analysis

We conducted a detailed study with a nematic liquid crystal (E7) coated in PEI surfactant at a concentration of 1 wt%, which showed a bipolar structure.[69] When we combined different concentrations of Tween-20 (0.2, 0.1, and 0.05 wt%) with PEI (1 wt%) and applied this mixture to coat LC droplets, we observed a radial configuration (homeotropics) under polarized optical microscopy (POM).[68] As an amphiphilic molecule, Tween-20 integrates into the PEI layer coating the LC droplets, altering the orientation of the LC molecules perpendicular to the director and enhancing birefringence under POM, with a central defect visible without cross polarizers.

From these combinations, we selected PEI/Tween-20 (1 wt% PEI and 0.05 wt% Tween-20) as the optimal continuous phase for producing LC droplets. To achieve monodispersed LC droplets, we employed a flow-focusing microfluidic device, setting the continuous phase (PEI/Tween-20 solution) flow rate to 20 μL min^{-1} and the dispersed phase (NLC) flow rate to 0.3 μL min^{-1} at room temperature. This setup yielded monodispersed LC droplets with an average diameter of 85 μm. The PEI coating on the droplet surface prevents collapse, while Tween-20 facilitates the transition from planar (radial) to homeotropic (bipolar) anchoring. Consequently, the LC

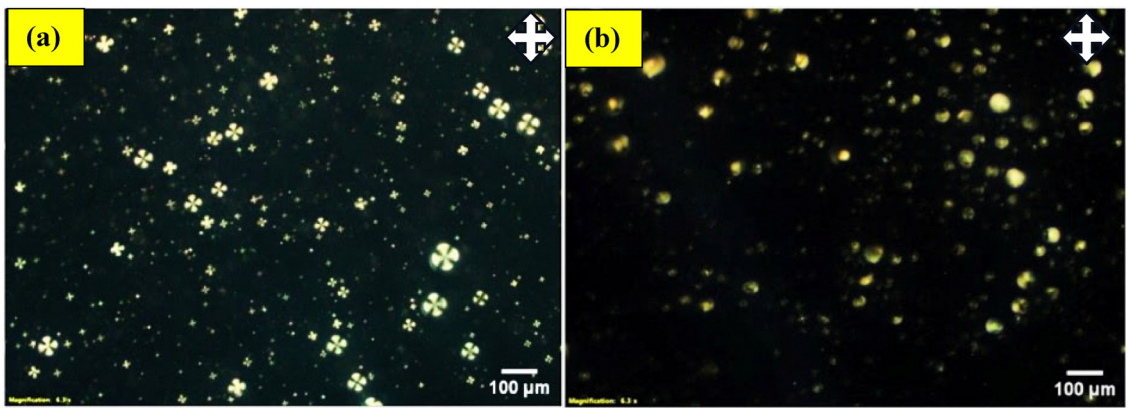

Fig. 4 POM images of LC droplets coated with PEI/Tween-20: (a) before and (b) after the addition of Hg^{2+} ions (59 mM) in a buffer solution at pH 4.

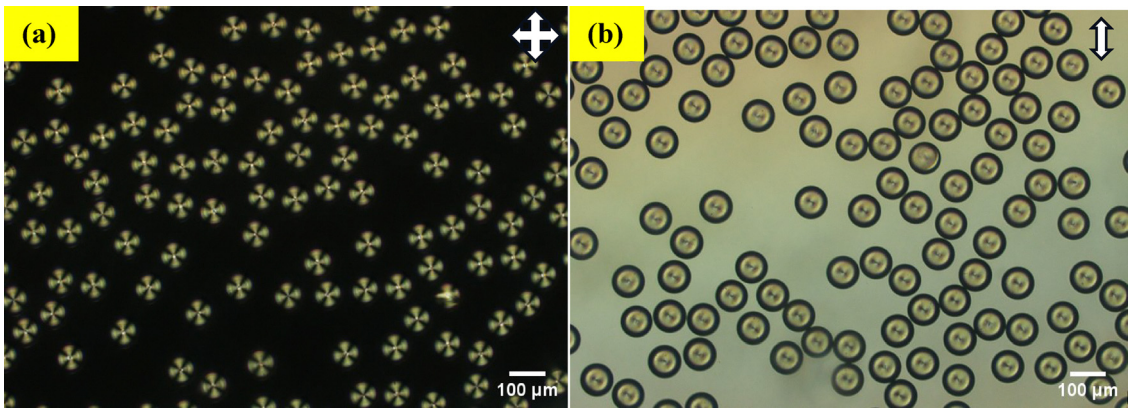

Fig. 5 POM images of PEI/Tween-20-coated LC droplets produced by a flow-focusing microfluidic device, showing an average droplet diameter of 85 μm in a homeotropic configuration: (a) with cross polarizers and (b) without cross polarizers.

droplets display a homeotropic configuration with an average diameter of 85 μm (measure under POM), as shown in Fig. 5.

3.3 Detection of mercury ion using $LC_{PEI/Tween\text{-}20}$ droplets

After confirming the homeotropic orientation of LC droplets coated with PEI/Tween-20 (1 wt% PEI, 0.05 wt% Tween-20) under polarized optical microscopy (POM), we proceeded to introduce an aqueous mercury ion solution to the PEI/Tween-20-coated LC droplets to observe their response. The time-lapse sequence of images captured under POM, as shown in Fig. 6 and 7(i)–(viii), alongside the attached video file, illustrates the dynamic changes in droplet configuration upon exposure to mercury ions.

Initially, the LC droplets displayed a well-defined homeotropic orientation with a fan-like structure, characteristic of their stable configuration in the absence of mercury ions. However, following the addition of mercury ions, the homeotropic orientation began to gradually transform. The fan-like structure diminished as the droplets adopted a bipolar configuration, signifying a planar alignment of the LC molecules within the droplets.

This shift from homeotropic to bipolar orientation is driven by the adsorption of mercury ions onto the surface of the $LC_{PEI/Tween\text{-}20}$ droplets. The mercury ions interact with the amine groups in the PEI layer, altering the surface anchoring conditions of the LC molecules. Consequently, this interaction disrupts the homeotropic alignment, promoting a planar configuration in response to mercury ion adsorption. This transition is clearly illustrated in Fig. 7, where the visual changes in droplet orientation provide a straightforward and label-free optical indicator of mercury ion presence, demonstrating the effectiveness of PEI/Tween-20-coated LC droplets for detecting mercury ions in an aqueous environment.

To confirm the specificity of $LC_{PEI/Tween\text{-}20}$ droplets for detecting Hg^{2+} ions in aqueous solutions, we investigated the orientational transition of these droplets upon the addition of various other metal ions (Mg^{2+}, Fe^{2+}, Cu^{2+}, Ca^{2+}, Cd^{2+}, Pb^{2+}, Zn^{2+}, and Na^{+}) to the sensor system. Even after 30 min at a concentration of 59 mM, none of these metal ions induced a structural transition in the $LC_{PEI/Tween\text{-}20}$ droplets, which retained their homeotropic configuration, as shown in Fig. 8(a)–(h). This indicates the selectivity and reliability of the sensor, as the $LC_{PEI/Tween\text{-}20}$ droplets consistently displayed a homeotropic structure for all tested ions except Hg^{2+}. In the presence of Hg^{2+} ions, however, a clear transition from homeotropic to planar structure was observed in the aqueous solution, as illustrated in Fig. 8(i).

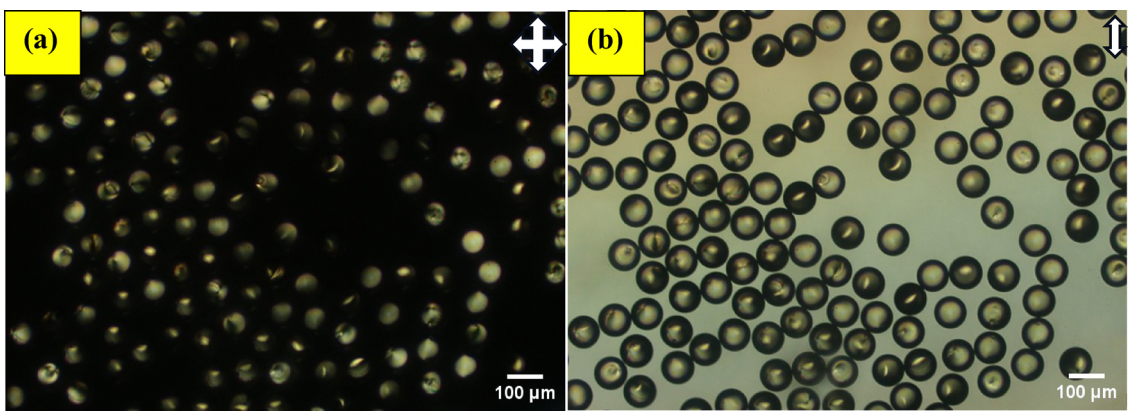

Fig. 6 POM images of LC droplets coated with PEI/Tween-20 after the addition of Hg^{2+} ion aqueous solution at a concentration of 59 mM: (a) with cross polarizers and (b) without cross polarizers.

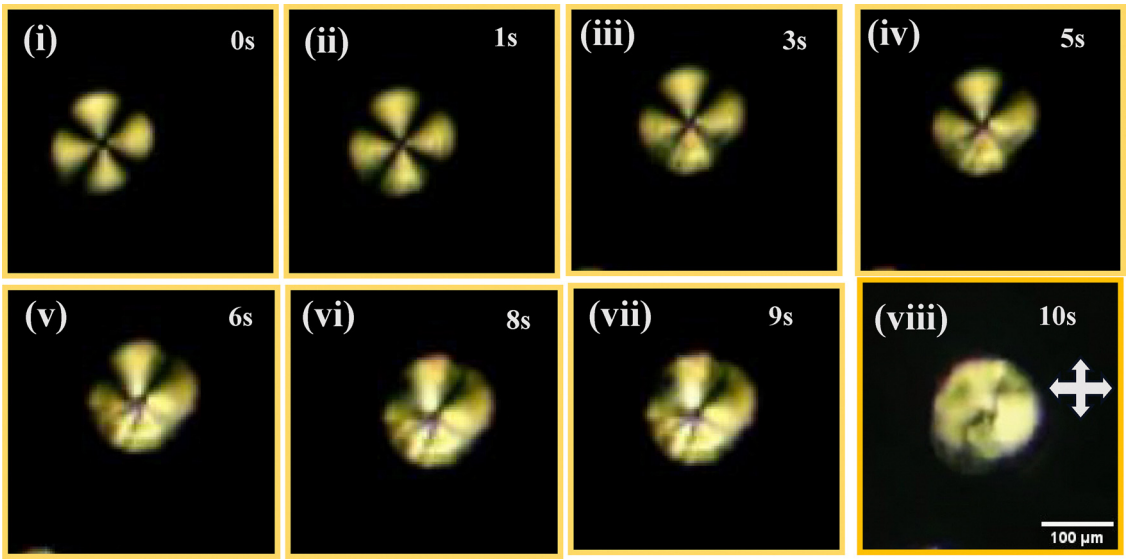

Fig. 7 POM images of LC droplets (85 μm diameter) coated with PEI/Tween-20, captured in transmission mode at intervals following the introduction of 40 μL of Hg^{2+} ion aqueous solution: (i) 0 s, (ii) 1 s, (iii) 3 s, (iv) 5 s, (v) 6 s, (vi) 8 s, (vii) 9 s, and (viii) 10 s.

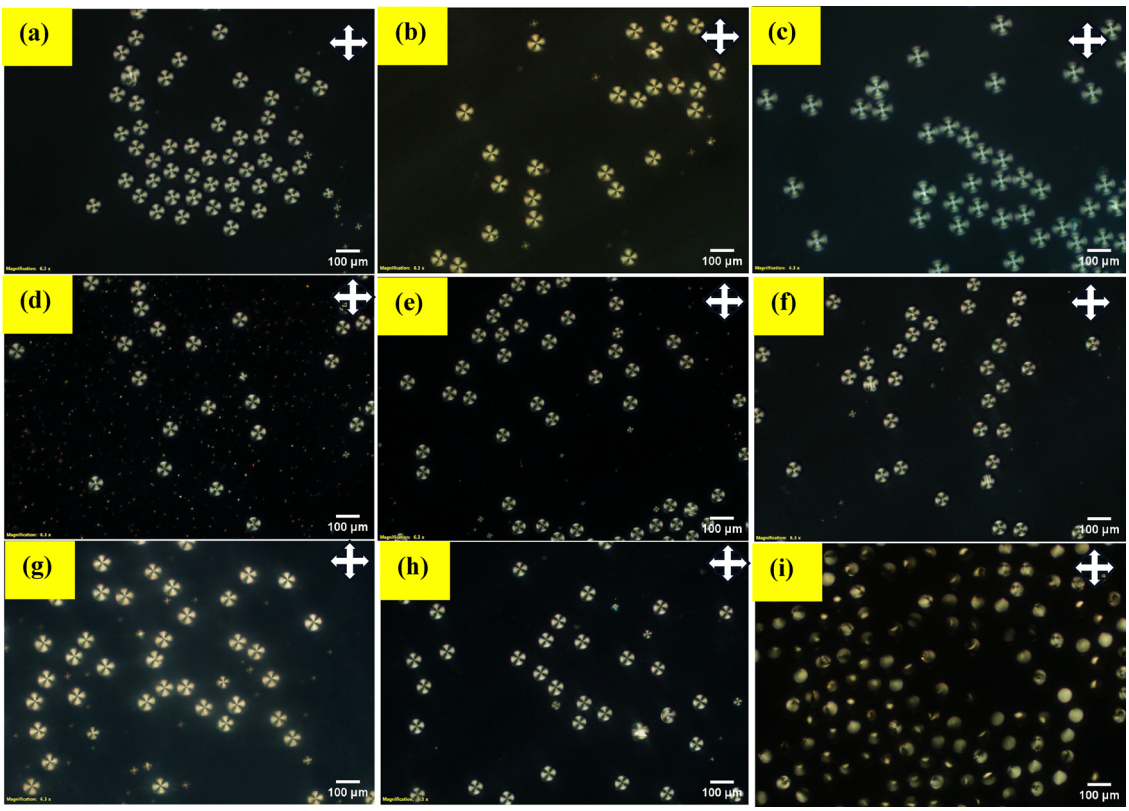

Fig. 8 POM images of $LC_{PEI/Tween\text{-}20}$ droplets after the addition of 59 mM aqueous solutions of various metal ions: (a) Mg^{2+}, (b) Fe^{2+}, (c) Cu^{2+}, (d) Ca^{2+}, (e) Cd^{2+}, (f) Zn^{2+}, (g) Pb^{2+}, (h) Na^{+}, and (i) Hg^{2+}.

To assess the sensor's performance in a complex ionic environment for real-time applications, we carefully studied a mixture of other metal ions (*e.g.*, Cu^{2+}, Fe^{2+}) in aqueous solution (tap water). In these mixed-ion environments, the $LC_{PEI/Tween\text{-}20}$ droplets showed no orientational transition, as illustrated in Fig. 9(a). However, upon introducing Hg^{2+} ions at a concentration of 59 mM to the same solution, the $LC_{PEI/Tween\text{-}20}$ droplets displayed a clear transition from homeotropic to

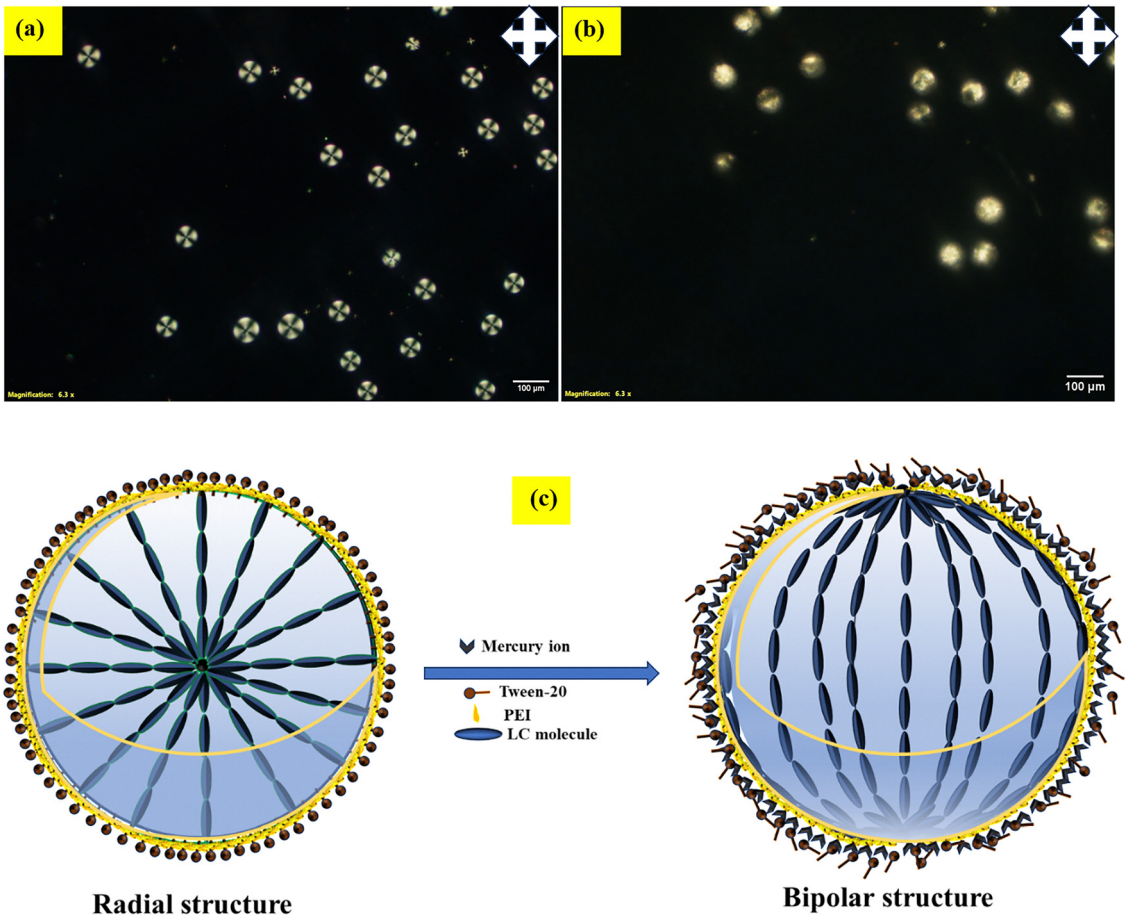

Fig. 9 (a) POM images of $LC_{PEI/Tween\text{-}20}$ droplets after addition of (a) Cu^{+2}, Fe^{+2} (b) Cu^{+2}, Fe^{+2}, Hg^{+2} ion (c) Schematic representation $LC_{\text{-}PEI/Tween\text{-}20}$ droplets of transition after addition of mercury ion.

planar orientation within 15 s. This result demonstrates that Hg^{2+} ions in aqueous solution can be effectively detected through the homeotropic-to-planar transition in LC droplets as shown in Fig. 9(b).

Driven by the particular sensitivity of $LC_{PEI/Tween\text{-}20}$ droplets to mercury ion adsorption, we sought to identify the fundamental detection mechanism. A PEI/Tween-20 surfactant layer covers the LC droplets; the surfactant consists in amine (NH_2) groups. These amine groups generate strong coordination complexes that enhance their attraction for metal ion by means of nitrogen atoms able to donate electrons.[70,71] This binding process reduces the tendency to form dative π-bonds between metal ion and nitrogen atoms, enabling two nitrogen atoms to coordinate with a single metal ion in solution. Here the formation of the Hg–amine complex disrupts the orientation of the liquid crystal droplets.

In this system, PEI acts both as a surfactant and as a chelating ligand for Hg^{2+} ions. Even minimal perturbation by mercury ions is sufficient to induce a transition in PEI/Tween-20-coated LC droplets from homeotropic to planar orientation. When Hg^{2+} ions are present in the aqueous solution, the $LC_{PEI/Tween\text{-}20}$ droplets transition from a homeotropic (radial) to a planar (bipolar) configuration, while with other metal ions, the droplets retain their radial orientation. This indicates strong specificity of the system for Hg^{2+} detection, attributed to the high binding affinity of the amine groups for mercury ions and also more adsorption power of PEI toward mercury ion (0.87 mmol g^{-1}) compare to the other metal ions (Mg^{2+}, Fe^{2+}, Cu^{2+}, Ca^{2+}, Cd^{2+}, Pb^{2+}, Zn^{2+}, and Na^{+}),[17,18] a finding consistent with other metal ions as shown in Fig. 8.

The proposed detection mechanism is illustrated schematically in Fig. 9(c). In the absence of Hg^{2+} or other metal ions (such as Mg^{2+}, Fe^{2+}, Cu^{2+}, Ca^{2+}, Cd^{2+}, Zn^{2+}, Pb^{2+}, and Na^{+}), the $LC_{PEI/Tween\text{-}20}$ droplets display a homeotropic orientation due to the presence of Tween-20 amphiphilic molecules on their surfaces. When Hg^{2+} ions are introduced, however, the orientation shifts from homeotropic (radial) to planar (bipolar). This shift results from the interaction between PEI and mercury ions, which displaces the amphiphilic molecules from the LC droplet surfaces. A video demonstrating this detection mechanism is available in ESI,† Video S1.

3.4 Detection of mercury ion by dye-doped interface method

This experiment provides clear evidence of the interactions between a coumarin dye and mercury ions on liquid crystal (LC) droplet surfaces. We sought to examine the nature of interactions by applying a coumarin dye in conjunction with an aqueous mercury ion solution to the surfaces of liquid crystal

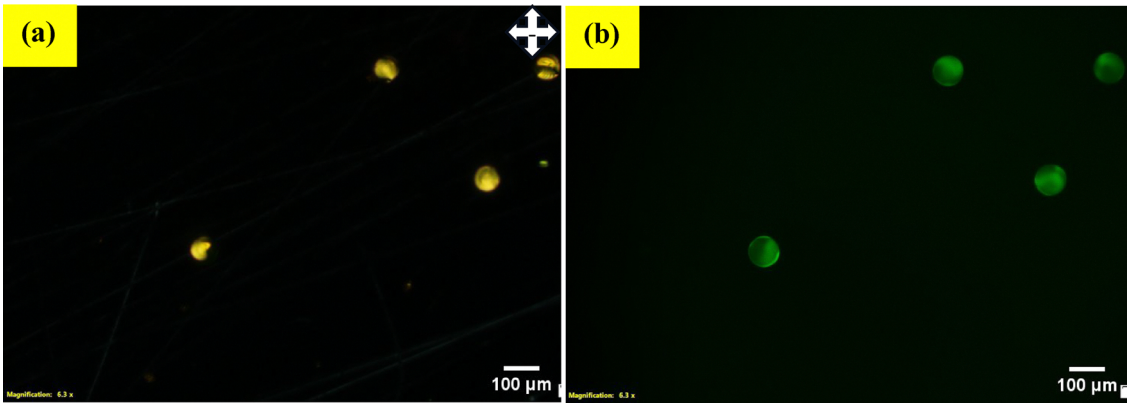

Fig. 10 POM images of $LC_{PEI/Tween\text{-}20}$ coated droplets with coumarin dye doped with mercury ions: (a) bright field, (b) fluorescence image.

droplets. Fluorescence microscopy revealed a significant finding: the coumarin dye efficiently adhered to the surfaces of the LC droplets, resulting in strong fluorescence emission. This effect may arise from the interaction between mercury ions and the $LC_{PEI/Tween\text{-}20}$-coated surfaces of the droplets, which appears to alter their orientation from homeotropic to planar. This change in orientation is illustrated in Fig. 10(a) and (b), which provides both bright-field and fluorescence pictures for comparison examination.

3.5 Raman spectroscopy studies

Fig. 11 shows the Raman spectrum, offering a comprehensive examination of the molecular interactions occurring when mercury ions attach to the surfaces of PEI/Tween 20-coated liquid crystal droplets. The peak at 2230 cm^{-1} is attributed to the stretching vibration of the carbonitrile (C≡N) bond.[72] This peak signifies the presence of carbonitrile groups, which are integral to the chemical composition of the droplets. The peak at 1607 cm^{-1} is indicative of the amide group, a component of the poly(ethylene amine) (PEI) coating on the LC droplets. This peak is significant as it exemplifies the impact of the coatings on the molecular structure, demonstrating how the amide group, through its unique vibrations, interacts with mercury ions. The amide functionality on the surface is essential for ion binding and anchoring, potentially stabilizing the droplet surface. The peak at 1289 cm^{-1} indicates the presence of biphenyl rings in the liquid crystal.[72] The biphenyl rings form the primary structure of the liquid crystal, providing stability and unique optical properties. The presence of this peak underscores the integrity of the liquid crystal structure, although its interaction with mercury ions, and offers insights on the alignment and orientation of the liquid crystal molecules. The peak at 1184 cm^{-1} signifies C–H stretching vibrations, typical of organic compounds.[73] The C–H stretching represents a fundamental vibrational mode, offering insight into the structural composition of the coating and the liquid crystal core. A subtle yet identifiable peak at 808 cm^{-1} indicates the ring breathing mode, a refined vibration within the aromatic rings. This peak signifies the interaction between the ring structures of the liquid crystal material and the mercury ions. The signal at 436 cm^{-1} is attributed to C–C stretching in the aliphatic chain. This peak highlights the importance of the aliphatic chain in maintaining the structural integrity of the coated LC droplets. The signal at 327 cm^{-1} unequivocally signifies the interaction of Hg^{2+} ions. This peak clearly indicates the vibrational response caused by the binding of mercury ions to the surfaces of the droplets. The observation confirms the successful binding of mercury ions, illustrating the specific chemical interaction between Hg^{2+} ions and the PEI/Tween 20-coated droplets. This peak is crucial, since it promptly illustrates the impact of mercury on the molecular architecture of the LC droplets, signifying a modification in their overall composition and behavior.

3.6 Limit of detection (LOD)

The minimum concentration of Hg^{2+} ions required to induce a change in the orientation of PEI/Tween-20-stabilized LC droplets from homeotropic to planar is known as the limit of detection (LOD). To test the detection capability in real water samples, we prepared Hg^{2+} ion solutions in distilled water, tap water and lake water. For response time measurements, LC droplets with a diameter of approximately 85 μm were used. In distilled water, the response time decreases from 161.33 s to 10 s as the Hg^{2+} concentration increases from 14.8 mM to 59 mM as shown in Fig. 12(a). Similarly, in tap water, the response time decreases from 224.33 s to 19 s with the same increase in concentration. The response time of lake water decreases from 42 s to 12.66 s as the concentration increases from 36.9 to 59 mM. This indicates that as the concentration of mercury ions decreases, the response time increases, as observed in the system's LOD for detecting mercury ions by repeating experiments with varying Hg^{2+} concentrations. In the optical images, a noticeable change in droplet configuration from homeotropic to planar is observed. Fig. 12(b) shows that for an aqueous mercury ion solution, as the volume increases from 40 μL to 160 μL, the LOD decreases from 14.73 mM to 4.71 mM. Fig. 12(b) shows that for an aqueous mercury ion solution, as the volume increases from 40 μL to 160 μL, the LOD decreases from 14.73 mM to 4.71 mM, while response time increases from 161.33 s to 516 s. This suggests that as the

volume of the Hg^{2+} ion solution increases, the LOD decreases, likely because a higher volume equates to more Hg^{2+} ions, thereby facilitating the transition of $LC_{PEI/Tween\text{-}20}$ droplets from homeotropic to planar orientation. The configuration transition from radial to bipolar was observed in PEI/Tween-20 droplets down to a mercury ion concentration of 4.71 mM. At concentrations below 4.71 mM (at volume 160 μL), no transition occurs even after 30 min of observation, indicating that this lower concentration does not contain enough Hg^{2+} ions to trigger the structural change.

Table 1 provides a comparison between the LC droplet sensing platforms for mercury ion detection. In this study, we used PEI/Tween-20 as a surfactant to produce LC droplets specifically for mercury ion detection in aqueous solutions. Other approaches, such as using aptamers, oligonucleotides, and amphiphilic dithiocarbamate (MeDTC), serve as

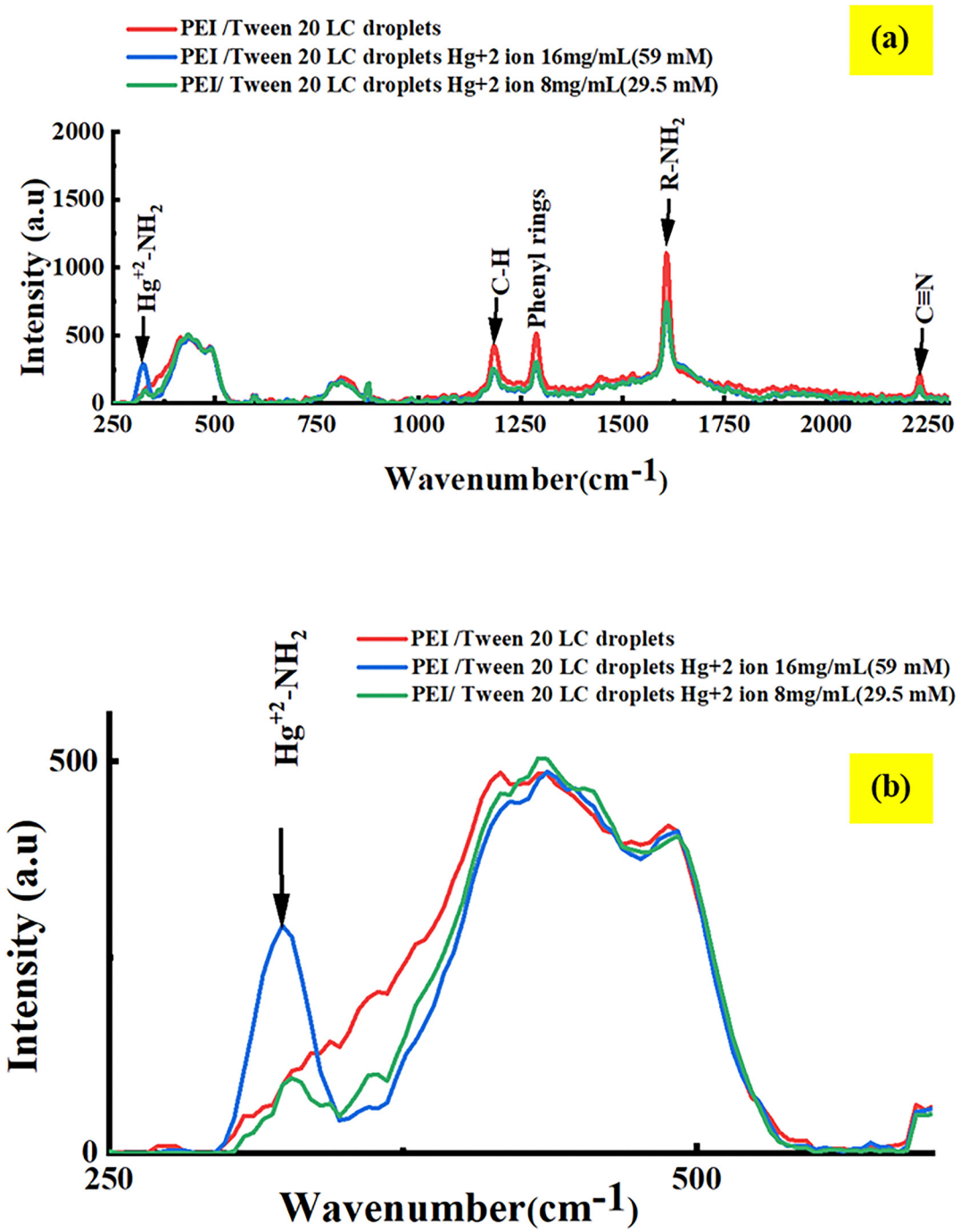

Fig. 11 (a) The Raman absorption spectra of $LC_{PEI/Tween\text{-}20}$ (red) and $LC_{PEI/Tween\text{-}20}$ with 59 mM (blue) and 29.5 mM (green) concentrations of mercury ion (b) zoom portion of Raman absorption spectra (250–560 cm^{-1}) represent Hg^{2+} ion and amine interaction.

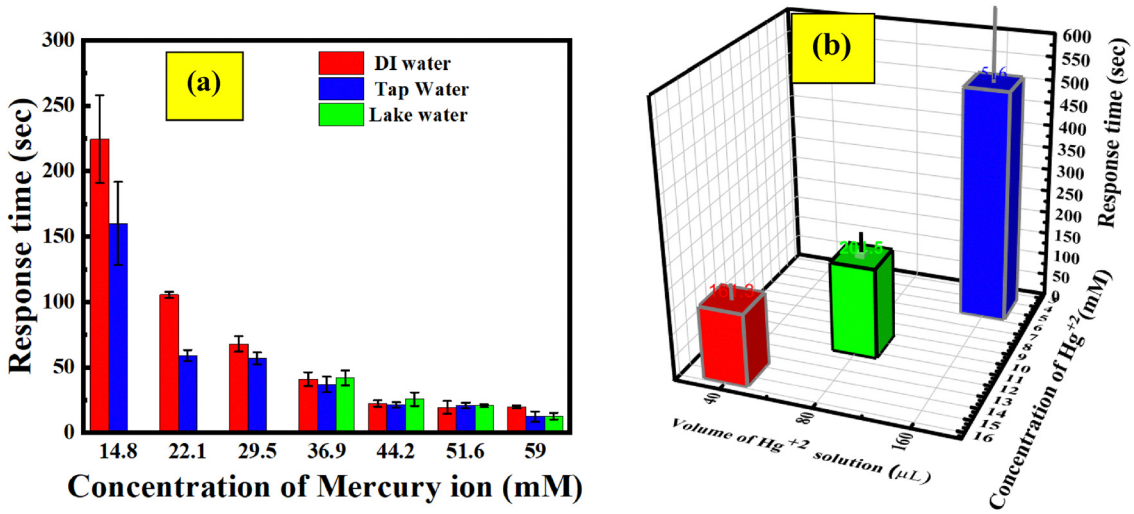

Fig. 12 (a) Response time of $LC_{PEI/Tween-20}$ droplets with an average diameter of 85 µm at different concentrations of Hg^{2+} ion. (b) Response time with respect to varying volumes of aqueous mercury ion solution at different concentration of mercury ion introduced into $LC_{PEI/Tween-20}$ droplets with standard deviation and error bar.

Table 1 Comparison between the LC droplet sensing platforms for mercury ion detection

LC materials	Sensing plat form	Detection probe	Principle	LOD	Response time	Ref.
4-Cyano-4′-pentylbiphenyl (5CB)	LC-solid	Oligonucleotide	Formation T–Hg^{2+}–T complex	0.1 nM	1 h	63
4-Cyano-4′-pentylbiphenyl (5CB)	LC-solid	5-(Pyridine-4yl)-2-(5-(pyridin-4-yl) thiophen-2-yl) thiazole (ZT)	Formation of ZT–Hg^{2+} complex	10 µM	10 min	64
4-Cyano-4′-pentylphenyl (5CB)	LC-solid	Amphiphilic dithiocarbamate (MeDTC)	MeDTC–Hg complex	0.5 µM	>5 min (tap water)	65
4-Cyano-4′-pentylphenyl (5CB)	LC-solid	Aptamer	Formation T–Hg^{2+}–T complex	100 pM	10 min	66
Nematic liquid crystal (E7)	**LC-aqueous interface**	**Surfactant PEI/Tween-20**	**PEI–Hg complex**	**4.71 mM**	**10 s**	**Current work**

recognition elements for mercury ion detection on LC-solid surfaces. In our work, we used PEI (1 wt%) and Tween-20 (0.05 wt%) as surfactants to create monodispersed LC droplets for mercury ion detection at the LC-aqueous interface, without the need for aptamer doping in the LC. Differences in detection limits and response times for mercury ions can be attributed to the diverse interactions between mercury ions and the detection probes, resulting in variable detection thresholds and response times.

Additionally, Table 1 provides a comparative analysis of liquid crystal (LC)-based biosensors for the detection of mercury ions (Hg^{2+}). In this study, LC droplets were employed without the incorporation of high-cost oligonucleotides to achieve selective detection of Hg^{2+} in drinking water. The response time was within 10 seconds, which is notably faster compared to other reported LC-based biosensors for Hg^{2+} detection. The PEI-coated LC droplets effectively reduced the concentration of Hg^{2+} due to the higher absorption capacity of PEI compared to other ions such as Mg^{2+}, Fe^{2+}, Cu^{2+}, Ca^{2+}, Cd^{2+}, Zn^{2+}, Pb^{2+}, and Na^{+}.[18] Moreover, the PEI/Tween-20 coated LC droplets facilitated the reduction of metal ion concentrations in the aqueous medium by adsorbing the ions onto their surfaces. In an aqueous solution, PEI/Tween-20 coated LC droplets show a dual nature for metal ions.

4. Conclusion

In conclusion, we have successfully developed a liquid crystal (LC)-based optical sensor for the selective detection of mercury (Hg^{2+}) ions in aqueous solutions. This system was realized by generating microdroplets of nematic LC coated with polyethyleneimine (PEI, 1 wt%) and Tween-20 (0.05 wt%), which initially exhibited a homeotropic orientation under polarized optical microscopy (POM). Upon exposure to Hg^{2+} ions, a distinct orientational change from homeotropic to planar alignment was observed at the aqueous interface. This transition is attributed to the strong interaction between the amine ($-NH_2$) groups of PEI and Hg^{2+} ions, resulting in the formation of a stable PEI–Hg^{2+} complex. These molecular-level interactions facilitated the selective recognition of Hg^{2+} and disrupted the LC alignment accordingly. Raman spectroscopy and fluorescence microscopy further validated these findings, confirming both the chemical interaction and the associated reconfiguration of the LC droplets. Using transmission-mode

POM, we characterized the sensor's performance, achieving a rapid response time of 10 s at a Hg^{2+} concentration of 59 mM, and a detection limit of 4.71 mM in distilled water. This label-free, straightforward, and cost-effective sensing platform enables efficient detection of mercury ions with high specificity. Moreover, the versatility of this approach suggests its potential for adaptation to detect other hazardous heavy metal ions, broadening its utility for environmental monitoring and public health applications.

Conflicts of interest

There are no conflicts to declare.

Data availability

The data will be made available on request to the corresponding author.

Acknowledgements

The authors would like to thank the Department of Physics and Central Instrument Facility (CRIF) at NIT Warangal for providing a Research facility. The authors acknowledge financial support from the Department of Biotechnology (DBT), New Delhi, India from Research grant no: BT/PR35841/MED/32/745/2020.

References

1 S. Ekino, M. Susa, T. Ninomiya, K. Imamura and T. Kitamura, Minamata Disease Revisited: An Update on the Acute and Chronic Manifestations of Methyl Mercury Poisoning, *J. Neurol. Sci.*, 2007, **262**(1–2), 131–144, DOI: 10.1016/j.jns.2007.06.036.

2 D. Hunter, R. R. Bomford and D. S. Russell, Poisoning by Methyl Mercury Compounds, *QJM*, 1940, **9**(3), 193–226, DOI: 10.1093/oxfordjournals.qjmed.a069154.

3 S. Bose-O'Reilly, K. M. McCarty, N. Steckling and B. Lettmeier, Mercury Exposure and Children's Health, *Curr. Probl. Pediatr. Adolesc. Health Care*, 2010, **40**(8), 186–215, DOI: 10.1016/j.cppeds.2010.07.002.

4 J. C. Clifton, Mercury Exposure and Public Health, *Pediatr. Clin. North Am.*, 2007, **54**(2), 237.e1–237.e45, DOI: 10.1016/j.pcl.2007.02.005.

5 K. N. Han, J. S. Choi and J. Kwon, Gold Nanozyme-Based Paper Chip for Colorimetric Detection of Mercury Ions, *Sci. Rep.*, 2017, **7**(1), 1–7, DOI: 10.1038/s41598-017-02948-x.

6 K. Leopold, M. Foulkes and P. Worsfold, Methods for the Determination and Speciation of Mercury in Natural Waters—A Review, *Anal. Chim. Acta*, 2010, **663**(2), 127–138, DOI: 10.1016/j.aca.2010.01.048.

7 S. Al Shehab and D. Patra, Binding of Metal Ions to the Curcumin Mediated Methoxy Polyethylene Glycol Thiol Conjugated Greenly Synthesized Gold Nanoparticles: A Fluorescence Spectroscopic Study, *J. Photochem. Photobiol., A*, 2021, **407**, 113083, DOI: 10.1016/j.jphotochem.2020.113083.

8 M. Wang, W. Feng, J. Shi, F. Zhang, B. Wang, M. Zhu, B. Li, Y. Zhao and Z. Chai, Development of a Mild Mercaptoethanol Extraction Method for Determination of Mercury Species in Biological Samples by HPLC-ICP-MS, *Talanta*, 2007, **71**(5), 2034–2039, DOI: 10.1016/j.talanta.2006.09.012.

9 D. Karunasagar, J. Arunachalam and S. Gangadharan, Development of a ''collect and Punch'' Cold Vapour Inductively Coupled Plasma Mass Spectrometric Method for the Direct Determination of Mercury at Nanograms per Litre Levels, *J. Anal. At. Spectrom.*, 1998, **13**(7), 679–682, DOI: 10.1039/A802132E.

10 N. Guo, G. Xu, Q. Zhang, P. Song and L. Xia, AgNPs Functionalized with Dithizone for the Detection of Hg2+ Based on Surface-Enhanced Raman Scattering Spectroscopy, *Plasmonics*, 2022, **17**(4), 1419–1426, DOI: 10.1007/s11468-022-01626-7.

11 A. Ono and H. Togashi, Highly Selective Oligonucleotide-Based Sensor for Mercury(II) in Aqueous Solutions, *Angew. Chem.*, 2004, **116**(33), 4400–4402, DOI: 10.1002/ange.200454172.

12 D. Wu, Q. Zhang, X. Chu, H. Wang, G. Shen and R. Yu, Ultrasensitive Electrochemical Sensor for Mercury (II) Based on Target-Induced Structure-Switching DNA, *Biosens. Bioelectron.*, 2010, **25**(5), 1025–1031, DOI: 10.1016/j.bios.2009.09.017.

13 X. Zhu, L. Chen, Z. Lin, B. Qiu and G. Chen, A Highly Sensitive and Selective ''Signal-on'' Electrochemiluminescent Biosensor for Mercury, *Chem. Commun.*, 2010, **46**(18), 3149, DOI: 10.1039/b926319e.

14 M. Li, Q. Wang, X. Shi, L. A. Hornak and N. Wu, Detection of Mercury(II) by Quantum Dot/DNA/Gold Nanoparticle Ensemble Based Nanosensor Via Nanometal Surface Energy Transfer, *Anal. Chem.*, 2011, **83**(18), 7061–7065, DOI: 10.1021/ac2019014.

15 G.-H. Chen, W.-Y. Chen, Y.-C. Yen, C.-W. Wang, H.-T. Chang and C.-F. Chen, Detection of Mercury(II) Ions Using Colorimetric Gold Nanoparticles on Paper-Based Analytical Devices, *Anal. Chem.*, 2014, **86**(14), 6843–6849, DOI: 10.1021/ac5008688.

16 M. Liu, Z. Wang, S. Zong, H. Chen, D. Zhu, L. Wu, G. Hu and Y. Cui, SERS Detection and Removal of Mercury(II)/Silver(I) Using Oligonucleotide-Functionalized Core/Shell Magnetic Silica Sphere@Au Nanoparticles, *ACS Appl. Mater. Interfaces*, 2014, **6**(10), 7371–7379, DOI: 10.1021/am5006282.

17 N. V. Jarvis and J. M. Wagener, Mechanistic Studies of Metal Ion Binding to Water-Soluble Polymers Using Potentiometry, *Talanta*, 1995, **42**(2), 219–226, DOI: 10.1016/0039-9140(94)00231-G.

18 A. Peñas-Sanjuán, R. Cruz-Sánchez, C. García-Gallarín, M. Pérez-Mendoza, R. López-Garzón and M. Melguizo, A Linear Free-Energy Relationship for the Prediction of Metal Ion Complexing Properties in Hybrid Carbon-Based Scavengers, *New J. Chem.*, 2023, **47**(27), 12883–12892, DOI: 10.1039/D3NJ01000G.

19 R. J. Carlton, J. T. Hunter, D. S. Miller, R. Abbasi, P. C. Mushenheim, L. N. Tan and N. L. Abbott, Chemical and Biological Sensing Using Liquid Crystals, *Liq. Cryst. Rev.*, 2013, **1**(1), 29–51, DOI: 10.1080/21680396.2013.769310.
20 Y. Bai and N. L. Abbott, Recent Advances in Colloidal and Interfacial Phenomena Involving Liquid Crystals, *Langmuir*, 2011, **27**(10), 5719–5738, DOI: 10.1021/la103301d.
21 R. R. Shah and N. L. Abbott, Principles for Measurement of Chemical Exposure Based on Recognition-Driven Anchoring Transitions in Liquid Crystals, *Science*, 2001, **293**(5533), 1296–1299, DOI: 10.1126/science.1062293.
22 N. A. Lockwood, J. K. Gupta and N. L. Abbott, Self-Assembly of Amphiphiles, Polymers and Proteins at Interfaces between Thermotropic Liquid Crystals and Aqueous Phases, *Surf. Sci. Rep.*, 2008, **63**(6), 255–293, DOI: 10.1016/j.surfrep.2008.02.002.
23 V. K. Gupta, J. J. Skaife, T. B. Dubrovsky and N. L. Abbott, Optical Amplification of Ligand-Receptor Binding Using Liquid Crystals, *Science*, 1998, **279**(5359), 2077–2080, DOI: 10.1126/science.279.5359.2077.
24 X. Cao, Y. Ye and S. Liu, Gold Nanoparticle-Based Signal Amplification for Biosensing, *Anal. Biochem.*, 2011, **417**(1), 1–16, DOI: 10.1016/j.ab.2011.05.027.
25 D. S. Miller, R. J. Carlton, P. C. Mushenheim and N. L. Abbott, Introduction to Optical Methods for Characterizing Liquid Crystals at Interfaces, *Langmuir*, 2013, **29**(10), 3154–3169, DOI: 10.1021/la304679f.
26 J. Park and N. L. Abbott, Ordering Transitions in Thermotropic Liquid Crystals Induced by the Interfacial Assembly and Enzymatic Processing of Oligopeptide Amphiphiles, *Adv. Mater.*, 2008, **20**(6), 1185–1190, DOI: 10.1002/adma.200702012.
27 S. Zhong and C.-H. Jang, Highly Sensitive and Selective Glucose Sensor Based on Ultraviolet-Treated Nematic Liquid Crystals, *Biosens. Bioelectron.*, 2014, **59**, 293–299, DOI: 10.1016/j.bios.2014.03.070.
28 F. Zuo, Z. Liao, C. Zhao, Z. Qin, X. Li, C. Zhang and D. Liu, An Air-Supported Liquid Crystal System for Real-Time Reporting of Host–Guest Inclusion Events, *Chem. Commun.*, 2014, **50**(16), 1857–1860, DOI: 10.1039/c3cc48885c.
29 X. Li, G. Li, M. Yang, L.-C. Chen and X.-L. Xiong, Gold Nanoparticle Based Signal Enhancement Liquid Crystal Biosensors for Tyrosine Assays, *Sens. Actuators, B*, 2015, **215**, 152–158, DOI: 10.1016/j.snb.2015.03.054.
30 V. Sharma, A. Kumar, P. Ganguly and A. M. Biradar, Highly Sensitive Bovine Serum Albumin Biosensor Based on Liquid Crystal, *Appl. Phys. Lett.*, 2014, **104**(4), 043705, DOI: 10.1063/1.4863740.
31 A. D. Price and D. K. Schwartz, DNA Hybridization-Induced Reorientation of Liquid Crystal Anchoring at the Nematic Liquid Crystal/Aqueous Interface, *J. Am. Chem. Soc.*, 2008, **130**(26), 8188–8194, DOI: 10.1021/ja0774055.
32 S. L. Lai, S. Huang, X. Bi and K.-L. Yang, Optical Imaging of Surface-Immobilized Oligonucleotide Probes on DNA Microarrays Using Liquid Crystals, *Langmuir*, 2009, **25**(1), 311–316, DOI: 10.1021/la802672b.
33 I. Verma, S. Sidiq and S. K. Pal, Poly(L-Lysine)-Coated Liquid Crystal Droplets for Sensitive Detection of DNA and Their Applications in Controlled Release of Drug Molecules, *ACS Omega*, 2017, **2**(11), 7936–7945, DOI: 10.1021/acsomega.7b01175.
34 X. Ding and K.-L. Yang, Antibody-Free Detection of Human Chorionic Gonadotropin by Use of Liquid Crystals, *Anal. Chem.*, 2013, **85**(22), 10710–10716, DOI: 10.1021/ac400732n.
35 V. J. Aliño, P. H. Sim, W. T. Choy, A. Fraser and K.-L. Yang, Detecting Proteins in Microfluidic Channels Decorated with Liquid Crystal Sensing Dots, *Langmuir*, 2012, **28**(50), 17571–17577, DOI: 10.1021/la303213h.
36 B. H. Clare and N. L. Abbott, Orientations of Nematic Liquid Crystals on Surfaces Presenting Controlled Densities of Peptides: Amplification of Protein−Peptide Binding Events, *Langmuir*, 2005, **21**(14), 6451–6461, DOI: 10.1021/la050336s.
37 L. Yang, M. Khan and S.-Y. Park, Liquid Crystal Droplets Functionalized with Charged Surfactant and Polyelectrolyte for Non-Specific Protein Detection, *RSC Adv.*, 2015, **5**(118), 97264–97271, DOI: 10.1039/C5RA15647E.
38 H. Maheshwari, P. M. Naveenkumar, R. K. Singh, L. Soni and K. P. Sharma, Charge Modulation at the Liquid Crystal Droplet-Aqueous Interface Enables Ultrasensitive, Nonspecific Protein Detection, *Small*, 2024, **20**(52), 2407077, DOI: 10.1002/smll.202407077.
39 S. Ranjan Pradhan, B. Gollapelli, R. Suguru Pathinti, R. Kandimalla and J. Vallamkondu, Optical Detection of Bovine Serum Albumin Using Charged Cholesteric Liquid Crystal Droplets Functionalized with Surfactant, *J. Mol. Liq.*, 2023, **386**, 122447, DOI: 10.1016/j.molliq.2023.122447.
40 I. Pani, S. Sil, R. Kaur, M. Devi and S. K. Pal, Dynamic Microparticle Assembly at the Interface of Chemoresponsive Liquid Crystal Droplets, *Anal. Chem.*, 2024, **96**, 3780–3786, DOI: 10.1021/acs.analchem.3c04555.
41 J. Hoogboom, K. Velonia, T. Rasing, A. E. Rowan and R. J. M. Nolte, LCD-Based Detection of Enzymatic Action, *Chem. Commun.*, 2006, (4), 434–435, DOI: 10.1039/B514048J.
42 D. Hartono, X. Bi, K. Yang and L. L. Yung, An Air-Supported Liquid Crystal System for Real-Time and Label-Free Characterization of Phospholipases and Their Inhibitors, *Adv. Funct. Mater.*, 2008, **18**(19), 2938–2945, DOI: 10.1002/adfm.200800424.
43 C.-Y. Chang and C.-H. Chen, Oligopeptide-Decorated Liquid Crystal Droplets for Detecting Proteases, *Chem. Commun.*, 2014, **50**(81), 12162–12165, DOI: 10.1039/C4CC04651J.
44 D. Liu and C.-H. Jang, A New Strategy for Imaging Urease Activity Using Liquid Crystal Droplet Patterns Formed on Solid Surfaces, *Sens. Actuators, B*, 2014, **193**, 770–773, DOI: 10.1016/j.snb.2013.12.033.
45 G.-R. Han, Y.-J. Song and C.-H. Jang, Label-Free Detection of Viruses on a Polymeric Surface Using Liquid Crystals, *Colloids Surf., B*, 2014, **116**, 147–152, DOI: 10.1016/j.colsurfb.2013.12.037.
46 S. Sivakumar, K. L. Wark, J. K. Gupta, N. L. Abbott and F. Caruso, Liquid Crystal Emulsions as the Basis of Biological Sensors for the Optical Detection of Bacteria and Viruses, *Adv. Funct. Mater.*, 2009, **19**(14), 2260–2265, DOI: 10.1002/adfm.200900399.

47 M. Khan and S.-Y. Park, General Liquid-Crystal Droplets Produced by Microfluidics for Urea Detection, *Sens. Actuators, B*, 2014, **202**, 516–522, DOI: **10.1016/j.snb.2014.05.115**.
48 J. Deng, X. Wang, W. Liang, D. Richardson, Q. Lu and J. Fang, Surface Modified Liquid Crystal Droplets as an Optical Probe for the Detection of Bile Acids in Microfluidic Channels, *Colloids Surf., A*, 2018, **542**, 52–58, DOI: **10.1016/j.colsurfa.2018.01.041**.
49 S. Sidiq, G. V. R. K. Prasad, A. Mukhopadhaya and S. K. Pal, Poly(L-Lysine)-Coated Liquid Crystal Droplets for Cell-Based Sensing Applications, *J. Phys. Chem. B*, 2017, **121**(16), 4247–4256, DOI: **10.1021/acs.jpcb.7b00551**.
50 T. Bera and J. Fang, Optical Detection of Lithocholic Acid with Liquid Crystal Emulsions, *Langmuir*, 2013, **29**(1), 387–392, DOI: **10.1021/la303771t**.
51 J. Deng, W. Liang and J. Fang, Liquid Crystal Droplet-Embedded Biopolymer Hydrogel Sheets for Biosensor Applications, *ACS Appl. Mater. Interfaces*, 2016, **8**(6), 3928–3932, DOI: **10.1021/acsami.5b11076**.
52 M. Khan and S.-Y. Park, Specific Detection of Avidin–Biotin Binding Using Liquid Crystal Droplets, *Colloids Surf., B*, 2015, **127**, 241–246, DOI: **10.1016/j.colsurfb.2015.01.047**.
53 K. Lee, K. C. Gupta, S. Y. Park and I. K. Kang, Anti-IgG-Anchored Liquid Crystal Microdroplets for Label Free Detection of IgG, *J. Mater. Chem. B*, 2016, **4**(4), 704–715, DOI: **10.1039/c5tb02131f**.
54 J. Kim, M. Khan and S. Y. Park, Glucose Sensor Using Liquid-Crystal Droplets Made by Microfluidics, *ACS Appl. Mater. Interfaces*, 2013, **5**(24), 13135–13139, DOI: **10.1021/am404174n**.
55 H. G. Lee, S. Munir and S. Y. Park, Cholesteric Liquid Crystal Droplets for Biosensors, *ACS Appl. Mater. Interfaces*, 2016, **8**(39), 26407–26417, DOI: **10.1021/acsami.6b09624**.
56 S. H. Yoon, K. C. Gupta, J. S. Borah, S.-Y. Park, Y.-K. Kim, J.-H. Lee and I.-K. Kang, Folate Ligand Anchored Liquid Crystal Microdroplets Emulsion for in Vitro Detection of KB Cancer Cells, *Langmuir*, 2014, **30**(35), 10668–10677, DOI: **10.1021/la502032k**.
57 Y. Choi, K. Lee, K. C. Gupta, S. Y. Park and I. K. Kang, The Role of Ligand-Receptor Interactions in Visual Detection of HepG2 Cells Using a Liquid Crystal Microdroplet-Based Biosensor, *J. Mater. Chem. B*, 2015, **3**(44), 8659–8669, DOI: **10.1039/c5tb01213a**.
58 W. Li, M. Khan, L. Lin, Q. Zhang, S. Feng, Z. Wu and J. Lin, Monitoring H_2O_2 on the Surface of Single Cells with Liquid Crystal Elastomer Microspheres, *Angew. Chem.*, 2020, **132**(24), 9368–9373, DOI: **10.1002/ange.202004326**.
59 M. Khan, W. Li, S. Mao, S. N. A. Shah and J. Lin, Real-Time Imaging of Ammonia Release from Single Live Cells *via* Liquid Crystal Droplets Immobilized on the Cell Membrane, *Adv. Sci.*, 2019, **6**(20), 1900778, DOI: **10.1002/advs.201900778**.
60 P. Bao, D. A. Paterson, P. L. Harrison, K. Miller, S. Peyman, J. C. Jones, J. Sandoe, S. D. Evans, R. J. Bushby and H. F. Gleeson, Lipid Coated Liquid Crystal Droplets for the On-Chip Detection of Antimicrobial Peptides, *Lab Chip*, 2019, **19**(6), 1082–1089, DOI: **10.1039/C8LC01291A**.
61 Q.-Z. Hu and C.-H. Jang, Liquid Crystal-Based Sensors for the Detection of Heavy Metals Using Surface-Immobilized Urease, *Colloids Surf., B*, 2011, **88**(2), 622–626, DOI: **10.1016/j.colsurfb.2011.07.052**.
62 G.-R. Han and C.-H. Jang, Detection of Heavy-Metal Ions Using Liquid Crystal Droplet Patterns Modulated by Interaction between Negatively Charged Carboxylate and Heavy-Metal Cations, *Talanta*, 2014, **128**, 44–50, DOI: **10.1016/j.talanta.2014.04.026**.
63 S. Yang, C. Wu, H. Tan, Y. Wu, S. Liao, Z. Wu, G. Shen and R. Yu, Label-Free Liquid Crystal Biosensor Based on Specific Oligonucleotide Probes for Heavy Metal Ions, *Anal. Chem.*, 2013, **85**(1), 14–18, DOI: **10.1021/ac302989h**.
64 C.-H. Chen, Y.-C. Lin, H.-H. Chang and A. S.-Y. Lee, Ligand-Doped Liquid Crystal Sensor System for Detecting Mercuric Ion in Aqueous Solutions, *Anal. Chem.*, 2015, **87**(8), 4546–4551, DOI: **10.1021/acs.analchem.5b00675**.
65 S. K. Singh, R. Nandi, K. Mishra, H. K. Singh, R. K. Singh and B. Singh, Liquid Crystal Based Sensor System for the Real Time Detection of Mercuric Ions in Water Using Amphiphilic Dithiocarbamate, *Sens. Actuators, B*, 2016, **226**, 381–387, DOI: **10.1016/j.snb.2015.11.077**.
66 P. T. K. Hong, K. Yun and C.-H. Jang, Liquid Crystal-Based Droplet Sensor for the Detection of Hg(II) Ions Using an Aptamer as the Recognition Element, *BioChip J.*, 2021, **15**(2), 152–161, DOI: **10.1007/s13206-021-00010-7**.
67 B. Gollapelli, A. K. Tatipamula, S. Dewanjee, R. S. Pathinti and J. Vallamkondu, Detection of Bile Acids Using Optical Biosensors Based on Cholesteric Liquid Crystal Droplets, *J. Mater. Chem. C*, 2021, **9**(39), 13991–14002, DOI: **10.1039/d1tc02801d**.
68 S. R. Pradhan, R. S. Pathinti, R. Kandimalla, K. Chithari, M. R. Veeramalla N and J. Vallamkondu, Label-Free Detection of Aβ-42: A Liquid Crystal Droplet Approach for Alzheimer's Disease Diagnosis, *RSC Adv.*, 2024, **14**(17), 12107–12118, DOI: **10.1039/d4ra00615a**.
69 V. J. Aliño, J. Pang and K. L. Yang, Liquid Crystal Droplets as a Hosting and Sensing Platform for Developing Immunoassays, *Langmuir*, 2011, **27**(19), 11784–11789, DOI: **10.1021/la2022215**.
70 J. Jia, G. J. Cheng, A. Wu and S. Luan, Novel Imprinted Polyethyleneimine Nano-Fluorescent Probes with Controllable Selectivity for Recognizing and Adsorbing Metal Ions, *RSC Adv.*, 2017, **7**(57), 36048–36055, DOI: **10.1039/c7ra04712f**.
71 J. J. Gooding, D. B. Hibbert and W. Yang, Review Electrochemical Metal Ion Sensors. Exploiting Amino Acids and Peptides as Recognition Elements, *Sensors*, 2001, **1**(3), 75–90.
72 P. Kalita, R. K. Singh and A. Bhattacharjee, Interactions Investigated by the Spectroscopic, Microscopic and Molecular Docking Studies for Liquid Crystal-Based Biosensor, *Liq. Cryst.*, 2022, **49**(3), 297–311, DOI: **10.1080/02678292.2021.1962423**.
73 P. Kalita, S. S. Shukla, R. K. Singh and A. Bhattacharjee, Potential Liquid Crystal-Based Biosensor Depending on the Interaction between Liquid Crystals and Proteins, *Spectrochim. Acta, Part A*, 2021, **254**, 119634, DOI: **10.1016/j.saa.2021.119634**.